Supplement of Atmos. Meas. Tech., 10, 3151–3174, 2017
https://doi.org/10.5194/amt-10-3151-2017-supplement

Atmospheric Measurement Techniques
Open Access
EGU

Supplement of

Calibration and evaluation of CCD spectroradiometers for ground-based and airborne measurements of spectral actinic flux densities

Birger Bohn and Insa Lohse

Correspondence to: Birger Bohn (b.bohn@fz-juelich.de)

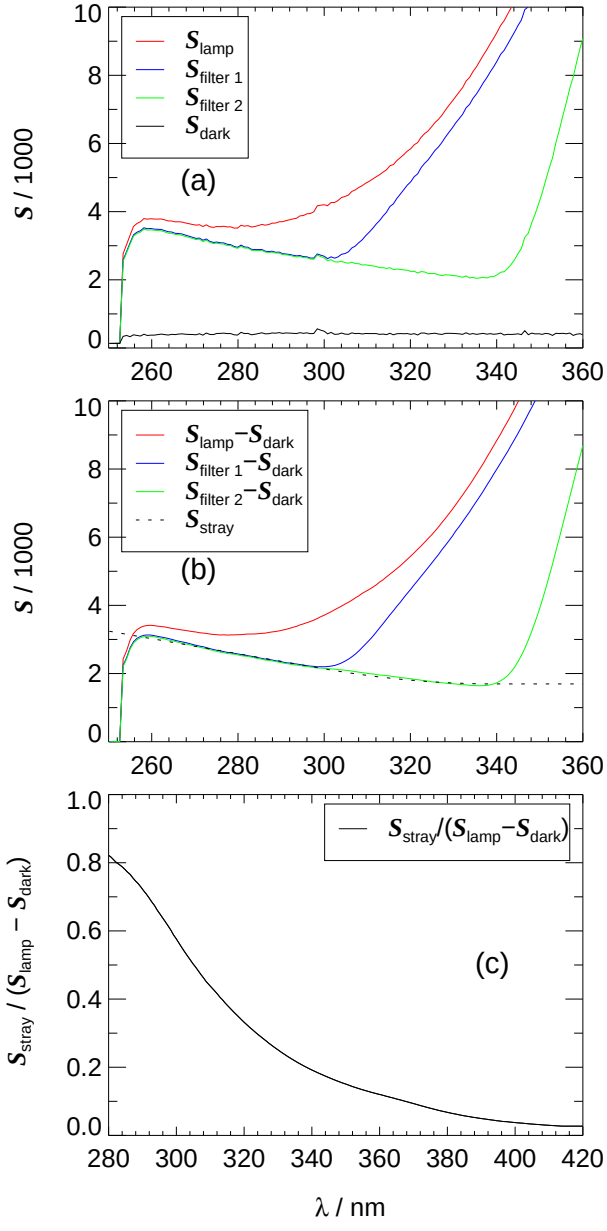

Figure S1: Example signals obtained during laboratory calibration measurements of instrument 45853 with 1000 ms integration time and two cutoff filters. Refer to Sect. 2.2.3 and caption of Fig. 6 for more details.

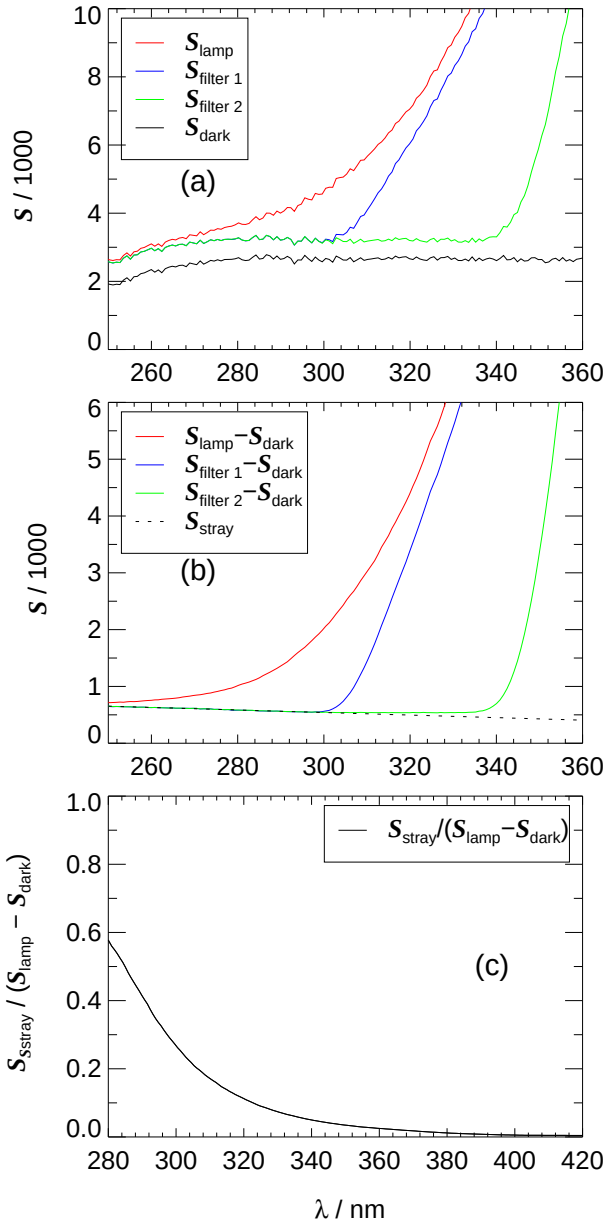

Figure S2: Example signals obtained during laboratory calibration measurements of instrument 62000 with 1000 ms integration time and two cutoff filters. Refer to Sect. 2.2.3 and caption of Fig. 6 for more details.

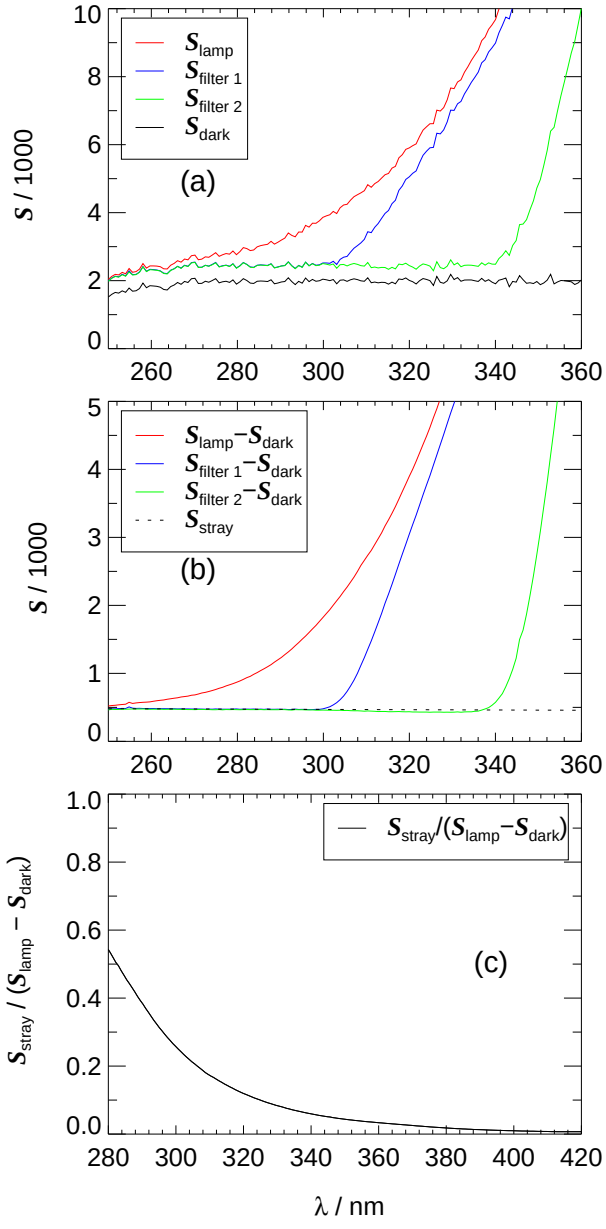

Figure S3: Example signals obtained during laboratory calibration measurements of instrument 62008 with 1000 ms integration time and two cutoff filters. Refer to Sect. 2.2.3 and caption of Fig. 6 for more details.

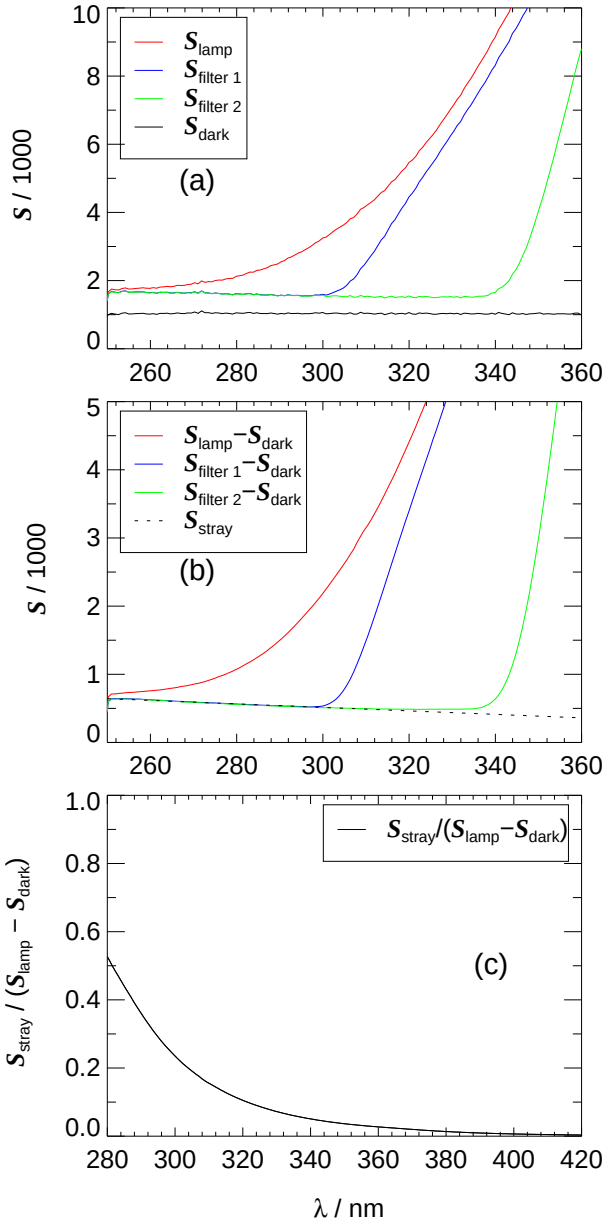

Figure S4: Example signals obtained during laboratory calibration measurements of instrument 85235 with 1000 ms integration time and two cutoff filters. Refer to Sect. 2.2.3 and caption of Fig. 6 for more details.

Table S1: Downward spectral actinic flux densities F_λ from radiative transfer calculations for selected wavelengths and solar zenith angles for an altitude of 0 km and an ozone column of 300 DU (left) and simulated noise equivalent actinic flux densities F_λ^{NE} of instrument 62001 for a maximum 300 ms integration time (right). The entry SZA>100° indicates dark conditions. See Tab. 4 for comparison.

λ / nm	300	350	400	450	500	550	600	650	300	350	400	450	500	550	600	650
SZA / deg	F_λ / 10^{12}cm^{-2}s^{-1}nm^{-1}								F_λ^{NE} / 10^{10}cm^{-2}s^{-1}nm^{-1}							
0	2.5	190	360	520	510	550	560	550	1.6	27	52	54	52	55	59	63
30	1.4	170	340	500	500	540	550	540	1.4	26	51	53	51	55	59	62
50	0.31	140	290	450	460	500	520	510	1.1	23	47	50	49	53	57	61
60	0.069	110	240	390	410	450	470	480	1.0	11	25	46	46	50	54	59
70	0.73[a]	64	160	280	310	350	370	400	1.0	8.8	20	40	40	45	49	54
80	0.16[a]	23	61	110	140	170	180	220	1.0	3.1	6.7	15	16	18	20	23
84	0.095[a]	12	28	50	60	70	77	100	1.0	2.2	4.7	5.3	10	12	13	16
88	0.042[a]	3.3	7.4	12	11	9.4	7.6	13	1.0	1.3	1.4	1.5	1.4	1.3	1.3	1.8
>100	0	0	0	0	0	0	0	0	1.0	0.6	0.4	0.3	0.3	0.3	0.3	0.4

[a] F_λ / 10^{10}cm^{-2}s^{-1}nm^{-1}

Table S2: Photolysis frequencies from radiative transfer calculations of downward spectral actinic flux densities for selected solar zenith angles at an altitude of 0 km and an ozone column of 300 DU (left) and simulated noise equivalent photolysis frequencies of instrument 62001 for a maximum 300 ms integration time (right). $j(\mathrm{O^1D})$ precisions in brackets were obtained by applying variable cutoff wavelengths (Fig. S5). The entry SZA>100° indicates dark conditions with zero spectral actinic flux densities. See Tab. 5 for comparison.

SZA /	photolysis frequency		noise equivalent photolysis frequency	
deg	$j(\mathrm{O^1D})$	$j(\mathrm{NO_2})$	$j(\mathrm{O^1D})$	$j(\mathrm{NO_2})$
0	3.73×10^{-5}	9.00×10^{-3}	1.1×10^{-7} (2.5×10^{-8})	1.2×10^{-6}
30	2.72×10^{-5}	8.38×10^{-3}	1.0×10^{-7} (2.1×10^{-8})	1.1×10^{-6}
50	1.33×10^{-5}	6.86×10^{-3}	1.0×10^{-7} (1.4×10^{-8})	9.6×10^{-7}
60	6.79×10^{-6}	5.46×10^{-3}	1.0×10^{-7} (9.6×10^{-9})	7.4×10^{-7}
70	2.37×10^{-6}	3.48×10^{-3}	1.1×10^{-7} (5.8×10^{-9})	4.8×10^{-7}
80	4.50×10^{-7}	1.27×10^{-3}	1.1×10^{-7} (4.0×10^{-9})	1.7×10^{-7}
84	1.75×10^{-7}	6.14×10^{-4}	1.1×10^{-7} (3.6×10^{-9})	9.7×10^{-8}
88	4.13×10^{-8}	1.63×10^{-4}	1.0×10^{-8} (2.5×10^{-9})	5.3×10^{-8}
>100	0.0	0.0	1.0×10^{-7} (2.5×10^{-9})	2.4×10^{-8}

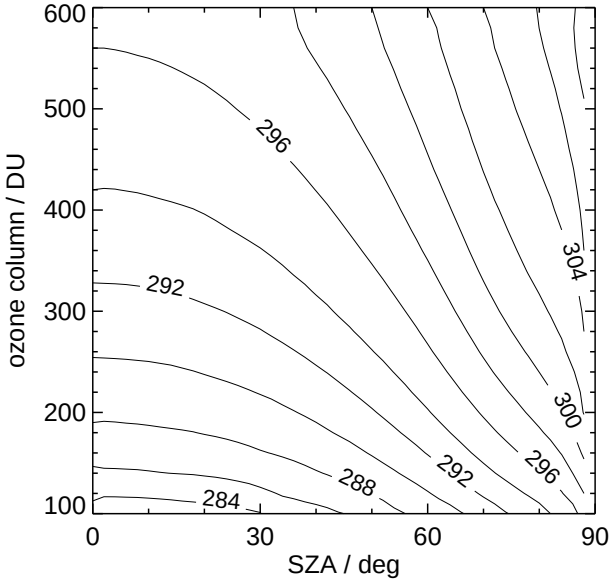

Figure S5: Contour plot of atmospheric cutoff wavelengths (nm) for an altitude of 0 km as a function of solar zenith angles (SZA) and ozone columns. The data were derived from radiative transfer calculations of downward clear sky spectral actinic flux densities defining a lower limit $F_\lambda \leq 5\times10^9 \mathrm{cm}^{-2}\mathrm{s}^{-1}\mathrm{nm}^{-1}$. See Fig. 12 for comparison.

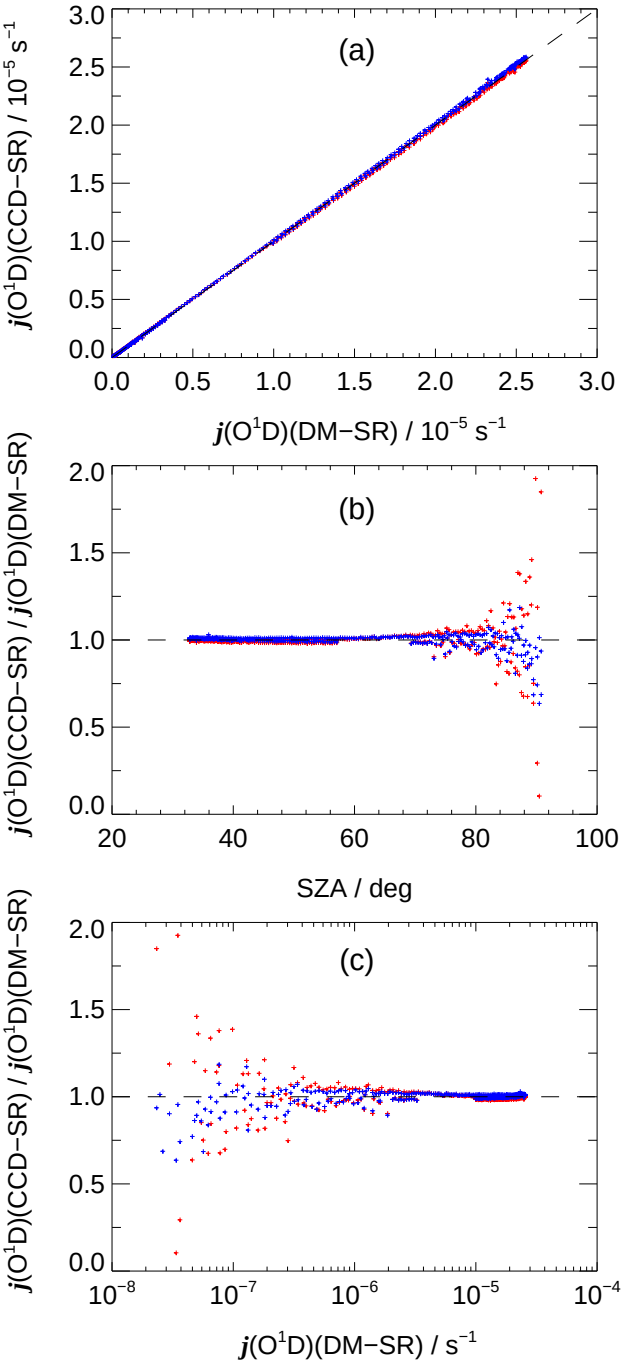

Figure S6: Comparison of $j(\mathrm{O}^1\mathrm{D})$ photolysis frequencies obtained on the ground with a double-monochromator based reference instrument (DM-SR) and instrument 62001. Measurements were made on 01 Aug 2013 at Jülich (Germany) under clear-sky conditions. Panel (a): correlation plot. Panel (b): ratios as a function of solar zenith angles. Panel (c): ratios as a function of reference values (DM-SR). Dashed lines indicate 1:1 relationships. Scatter in the ratios towards large SZA (middle panels) and low $j(\mathrm{O}^1\mathrm{D})$ (lower panels) is caused by different detection limits. Blue and red data points were obtained when spectral actinic flux densities below cutoff wavelengths were set to zero and not set to zero, respectively. See Fig. 18 for a typical comparison including more variable, cloudy conditions.

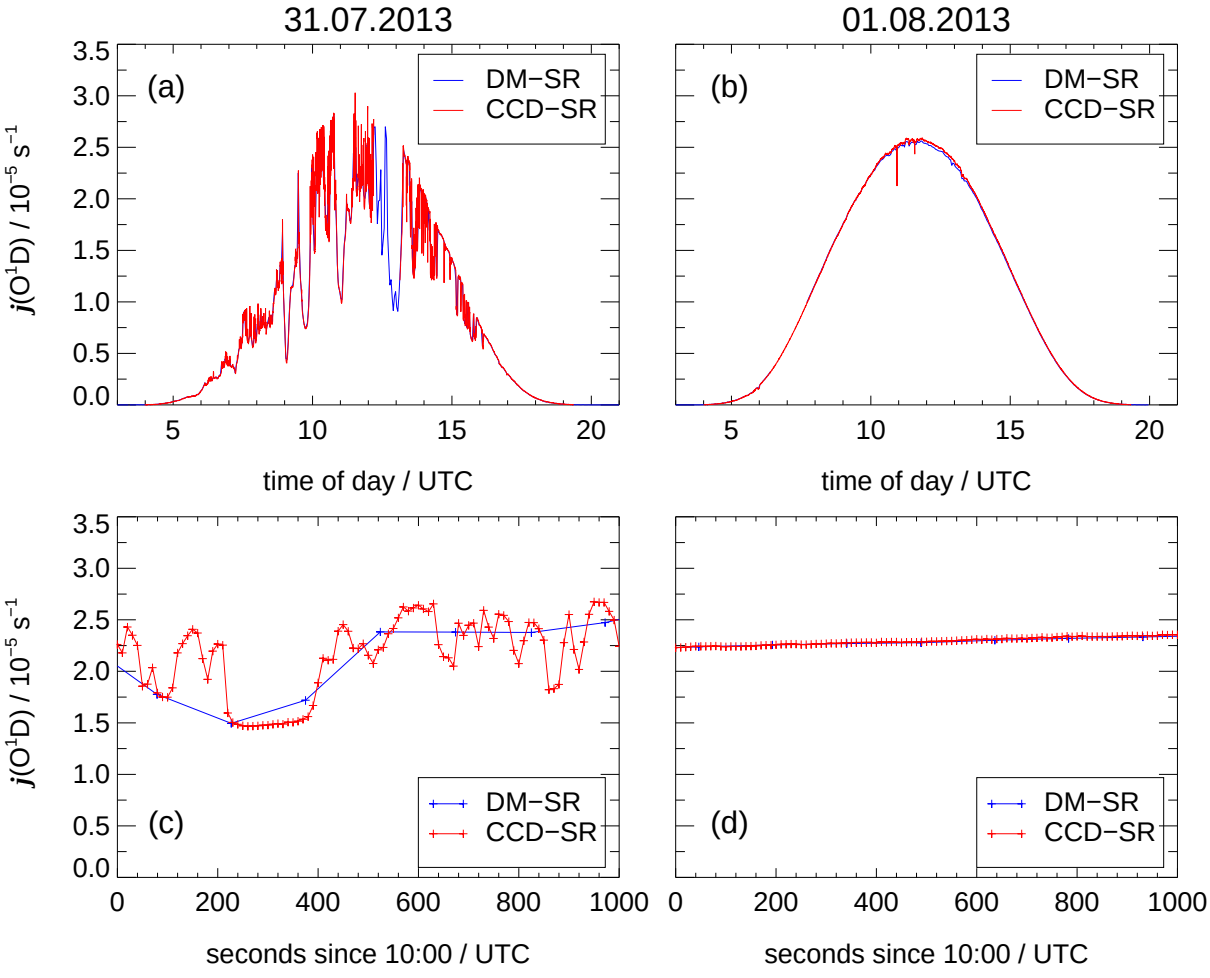

Figure S7: Comparison of $j(O^1D)$ photolysis frequencies obtained on the ground at Jülich (Germany) with a double-monochromator based reference instrument (DM-SR) and instrument 62001 (CCD-SR). Measurements of two successive days with broken cloud conditions in panel (a) (31 July) and clear-sky conditions in panel (b) (01 Aug 2013) are shown. Missing data indicate calibration periods for the CCD-SR in panel (a) and the DM-SR in panel (b). The lower panels (c) and (d) show 1000 s periods for each day to demonstrate the effects of different instrument time resolutions (≈150 s and 10 s, respectively). There is no synchronization issue on the clear-sky day while for the broken cloud conditions deviations can go in both directions.